School of Mathematical
and Physical Sciences

University of

Department of Mathematics and Statistics

Preprint MPS-2011-18

15 October 2012

A High Frequency *hp* Boundary Element Method for Scattering by Convex Polygons

by

D.P. Hewett, S. Langdon, J.M. Melenk

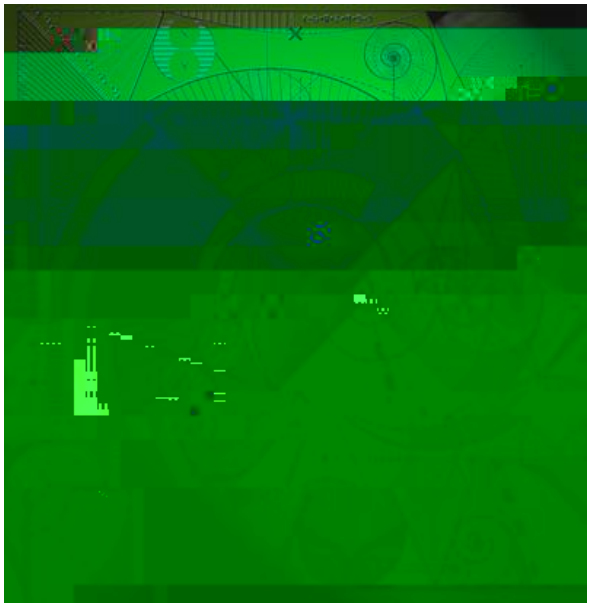

we study its properties and performance by numerical experiments backed up by rigorous numerical analysis. We show that our algorithm is exponentially convergent as a function of $p\overline{N}$, where N is the number of degrees of freedom, for fixed wavenumber k ($k = 2 f/c$ where f is the frequency and c the wave speed). More importantly (and it is for this property that the hybrid approach is key) our algorithm provably achieves any desired accuracy, uniformly over all wave numbers k, provided N increases logarithmically with k. These results improve on the h-version Galerkin BEM for the identical problem in [14], which is only algebraically convergent, and we note that the most sophisticated algorithm to date [20] for smooth 2D convex obstacles, while accurate for N and k large, is not convergent as $N \to \infty$ for k fixed.

Our results go beyond those of previous authors in terms of analysis in a number of important respects. Firstly, these are the first numerical analysis results for a hybrid approach which make explicit the dependence of all constants in the error estimates on the wavenumber k and both the h and p discretisation parameters. Secondly, this is the first numerical analysis for a bounded obstacle scattering problem which establishes that it is sufficient to increase N proportional to powers of $\log k$ to maintain accuracy as $k \to \infty$. The best previous result for smooth convex obstacles ([42], refining results in [20]) establishes that it is sufficient to increase N slightly faster than $k^{1/9}$ to retain accuracy, while the analysis in [14], when completed by the coercivity estimates of [42] and the estimates in §4 below, also requires a mild algebraic growth in N as $k \to \infty$ to maintain accuracy. (We note however that the hybrid h-version BEM proposed in [27], for the special problem of scattering in a half-plane with impedance boundary conditions, is shown in [27] to achieve any required accuracy uniformly in the wavenumber with N independent of k.)

We note that the hp-BEM we describe in this paper was briefly sketched in [35]; in this paper we describe the method in detail, provide a rigorous derivation of error estimates in the Galerkin solution, and demonstrate that our theoretical
achieved by the BEM in practice. We also demonstrate theoretically and numerically how the error in the BEM solution depends on the scatterer geometry. Our method

and $u^s := u - u^i$ satisfies the Sommerfeld radiation condition (see e.g. [12, (2.9)]). It follows from standard arguments connecting formulations in classical function spaces to those in a Sobolev space setting (see e.g. [17, Theorem 3.7] and [12, p. 107]) that if u satisfies the above BVP then also $u \in H^1_{\mathrm{loc}}(D)$, and, from standard elliptic regularity results, it follows moreover that u is C^1 up to the boundary of ∂D, excluding the corners of the polygon [12, Lemma 2.35].

Next we state our integral equation formulation. From [32, Theorems 7.15 and 9.6], for details see [14], we observe that if u satisfies the BVP then a form of Green's representation theorem holds, namely (cf. also [12, (2.107)])

$$u(x) = u^i(x) - \int_\Gamma \Phi_k(x,y)\frac{\partial u}{\partial n}(y)\,ds(y), \qquad x \in D, \tag{2.3}$$

where $\Phi_k(x,y) := (i/4)H_0^{(1)}(k|x-y|)$ is the fundamental solution for (2.2) and $\partial u/\partial n \in L^2(\Gamma)$ [12, Theorem 2.12], with n the unit normal directed into D. Furthermore, the BVP can be reformulated as a BIE for $\partial u/\partial n \in L^2(\Gamma)$, taking the form

$$A\frac{\partial u}{\partial n} = f, \tag{2.4}$$

where $f \in L^2(\Gamma)$ and $A : L^2(\Gamma) \to L^2(\Gamma)$ are specified next (for details see [12, §2]).

Classical combined potential formulation. In the standard combined potential formulation (e.g. [18], [12, (2.114) and (2.69)]),

$$A = A_k := \frac{1}{2}I + D_k' - iS_k,$$

and $f = \partial u^i/\partial n - iu^i$, where I is the identity operator,

$$S_k\varphi(x) := \int_\Gamma \Phi_k(x,y)\varphi(y)\,ds(y), \qquad x \in \Gamma, \quad \varphi \in L^2(\Gamma),$$

is the single-layer potential,

$$D_k'\varphi(x)$$

Properties of the boundary integral operators. For both formulations the following lemma holds provided is Lipschitz and $j\ j \quad Ck$ for the standard formulation. Here and for the remainder of this paper $C > 0$ denotes a constant whose value may change from one occurence to the next, but which is always independent of k, although it may (possibly) be dependent on the geometry of . We use C_j, c_j, k_j, etc., for $j = 0;1;2;:::$, to denote speci c constants whose value remains the same throughout the paper.

Lemma 2.1 ([11, Theorem 3.6], [42, Theorem 4.2]). *Assume that is a bounded Lipschitz domain and $k_0 > 0$. For the case $A = A_{k;}$ assume additionally $j\ j \quad Ck$. Then for both $A = A_k$ and $A = A_{k;}$ there exists a constant $C_0 > 0$, independent of k, such that*

$$kAk_{L^2(\ )} \quad C_0 k^{1=2}; \qquad k \quad k_0:$$

on each of the sides of the polygon, which we now consider. The results that follow in this section are for the case of a convex polygon.

We first define some notation. We label the corners of the polygon counterclockwise by P_j, $j = 1,\ldots,n_s$, where n_s is the number of sides. In addition, we set $P_{n_s+1} := P_1$, and, for $j = 1,\ldots,n_s$, denote the side between the corners P_j and P_{j+1} by Γ_j. We represent the point $x \in \Gamma$, whose arc-length measured counterclockwise around Γ from P_1 is s, parametrically by

$$x(s) = P_j + (s - \Sigma_{j-1})\frac{P_{j+1} - P_j}{L_j}; \quad \text{for } s \in [\Sigma_{j-1}, \Sigma_j], \quad j = 1,\ldots,n_s, \tag{3.1}$$

where $L_j = |P_{j+1} - P_j|$ is the length of the side Γ_j, and $\Sigma_j := \sum_{m=1}^{j} L_m$, $j = 1,\ldots,n_s$, denotes the arc-length distance from P_1 to P_{j+1}. We also set $\Sigma_0 = 0$, and denote the total length of Γ by $L := \Sigma_{n_s}$. We say that a side Γ_j is illuminated by the incident wave if $d \cdot n < 0$ on Γ_j, and is in shadow if $d \cdot n \geq 0$ on Γ_j. We denote by α_j the exterior angle at the corner P_j

Theorem 3.2. *The functions $v_j(s)$, $j = 1,\dots,n_s$, are analytic in the right half-plane* $\mathrm{Re}[s] > 0$, *where they satisfy the bounds*

$$|v_j(s)| \le \begin{cases} C_j M |ks|^{\alpha_j}; & 0 < |s| \le 1/k; \\ C_j M |ks|^{1/2}; & |s| > 1/k; \end{cases} \tag{3.5}$$

where α_j^+, $\alpha_j \in (0, 1/2)$ are given by $\alpha_j^+ := 1/2 - \alpha_j$ and $\alpha_j := 1/2 - \alpha_{j+1}$ and M by

$$M := \sup_{x \in D} |u(x)|. \tag{3.6}$$

For $j = 1,\dots,n_s$, the constants C_j^+ depend only on c and α_j, and the constants C_j depend only on c and α_{j+1}.

Remark 3.3. *The dependence of the constant M on the wavenumber k is not yet fully understood. In x4 we prove that, when Ω is a star-like polygon, $M = O(k^{1/2}\log^{1/2} k)$ as $k \to \infty$. However, it is plausible, and supported by numerical experiments, that in fact $M = O(1)$ as $k \to \infty$ in this case (and indeed for a more general class of polygons, see [13] for details).*

Bounds on the derivatives of the functions $v_j(s)$ for $s \in (0, \infty)$ have previously been derived in [14, Theorem 3.2, Corollary 3.4]. Here we show that it is possible to understand not just the behaviour of $v_j(s)$ for $s > 0$ but also to understand the behaviour of the analytic continuation of $v_j(s)$ into the complex plane. This will be an essential component of our *hp* analysis, which follows in x5, but may also be of wider interest, as indicated in the Introduction. The proof of Theorem 3.2 relies on a number of intermediate results. We first note the following:

Lemma 3.4. *The function $\Phi(z)$ is analytic in the half-plane* $\mathrm{Re}[z] > 0$, *with*

$$|\Phi(z)| \le \frac{2}{|z|^{3/2}} + \frac{1}{|z|^{1/2}} + \sqrt{\frac{\pi}{2}}; \qquad \mathrm{Re}[z] > 0. \tag{3.7}$$

Proof. By standard properties of the Hankel function $H_1^{(1)}(z)$ (see e.g. [1, (10.7.2), (10.7.8)]), $\Phi(z)$ is analytic in the cut z-plane, with branch cut along the negative real axis. By [37, equation (12.32)],

$$\Phi(z) = \frac{2i}{\pi}\int_0^\infty (t^2 - 2it)^{1/2} e^{-zt}\,dt; \qquad \mathrm{Re}[z] > 0; \tag{3.8}$$

where the branch of $(t^2 - 2it)^{1/2}$ is chosen so that $\mathrm{Re}\,(t^2 - 2it)^{1/2} \ge 0$ for $t > 0$. The integral in (3.8) is a parametrization of the contour integral

$$I(z) := \int_{\Gamma_0}

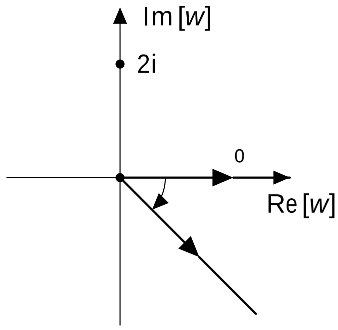

Fig. 3.1. *The contours* $_0$ *and* .

21]TJ/F10 6.9738 Tf 4.312 -1.494 Td [( )

so that

$$|I(z)| \int_0^{\infty} R e^{\ rR} \, dR + \frac{p}{2} \int_0^{\infty} R^{1=2} e^{\ rR} \, dR = \frac{1}{r^2} + \frac{p}{p \overline{2} r^{3=2}};$$

and the result follows. □

We now consider the solution behaviour near the corners.

Lemma 3.5. *Suppose that* $x \ 2 \ D$ *satis es* $|x \quad P_j| =: r \ 2 \ (0; 1=k]$. *Then there exists a constant* $C > 0$*, depending only on* $_j$ *and* c *, such that (with* M *given by (3.6))*

$$|u(x)| \quad CM(kr)^{\ = \ j}:$$

Proof. Let $(r; \ )$ be polar coordinates local to a corner P_j, chosen so that the side $_{j \ 1}$ lies on the line $= 0$ and the side $_j$ lies on the line $= \ _j$. For $R > 0$ let $G_R \quad \overline{D}$ denote the set of points with polar coordinates $f(r; \ ) : 0 < r < R; 0$ $_j g$. With $R_j := \min f L_{j \ 1}; L_j; \ =(2k) g$, it follows from [14, Theorem 2.3] and [14, (3.14)] that, for $0 < R < R_j$,

$$|u(x)| \quad \frac{2M(r=R)^{\ = \ j}}{\cos kR \ \ 1 \quad (r=R)^{\ = \ j}}; \quad x \ 2 \ G_R: \tag{3.9}$$

$_j$u

Now choose $R = 3R_j=4$, and suppose that $0 < r < R_j=2$. Then, since $\min f c \ ; \ =2 g$ BJ/F1 8.9620503 -11.955 Td [(k)]( )]TJ/F7738 Tf 13.474 -2.616 Td [(1.6)]TJ/F7 6.9738 Tf 8.391 0 Td [( )]TJ/F9 4.9813 Tf 5.687 -0.997 159
$kR_j \quad =2$, (3.9) implies that

$$|u(\qquad 2 \qquad f c \ ; \ =2$$

Proof. (Proof of Theorem 3.2.) The analyticity of $v_j(s)$ in $\mathrm{Re}[s] > 0$ is clear from (3.3){(3.4) and Lemma 3.4. To prove the bounds (3.5) for v_j^+ (the proof for v_j goes analogously and will be omitted here), we first note that

$$|v_j^+(s)| \le \frac{k^2}{2} \int_0^{1} |\chi(k(s+t))| |u(y_j(t_{j-1}) - t))| \, dt. \tag{3.10}$$

If $0 < |s| \le 1/k$ then we split the integral in (3.10) into a sum of two integrals, the first over $t \in (0, 1/k)$ and the second over $t \in (1/k, 1)$. For the second integral, Lemma 3.4 implies that, since $\mathrm{Re}[s + t$ over L_j/F11 9.9626 Tf 2.768 0 Td [( )]TJ/F7 6.9738 Tf 6.003 0 Td [(()]TJ/F11

(convex or non-convex). This result appears to be new, and could be used to improve the estimates of [14] directly, as well as being crucial to the *k*-explicit error analysis of our *hp* scheme which follows in *x*6. We begin with the following estimate of the norm of the single-layer potential operator in the domain.

Lemma 4.1.

Hence

$$k \quad {}_k(x;\ )k^2_{L^2(\ )} \quad \frac{5\hat{c}^2}{8\log 2}k^{\ 1}\sum_{j=1}^{N_s}\log(2+kL_j) \quad \frac{5\hat{c}^2}{8\log 2}k^{\ 1}n_s\log(2+kL\ );$$

and, recalling (4.2), the result follows. □

Next, we require a bound on the norm of $@u=@n$.

Lemma 4.2. *For a star-like Lipschitz scatterer,*

$$\frac{@u}{@n}_{L^2(\ )} \quad \frac{L^{1=2}(1+4k\,\mathrm{diam}\ )}{\mathrm{ess\,inf}_{x2}\ (x\ \ n(x))};\quad k>0:$$

Proof. By (2.4),

$$\frac{@u}{@n}_{L^2(\ )} \quad A^{\ 1}{}_{L^2(\ )}kfk_{L^2(\ )}; \tag{4.4}$$

and applying Lemma 2.2 with $A = A_k$, and recalling Remark 2.4, we have

$$A^{\ 1}{}_{L^2(\ )} \quad 2=\mathrm{ess\,inf}_{x2}\ (x\ \ n(x));\quad k>0: \tag{4.5}$$

It remains to bound $kfk_{L^2(\ )}$, where $f(x) = x \quad ru^i(x) \quad i\hat{}u^i(x)$ and $\hat{} = kjxj + i=2$ (where is star-like with respect to the origin of our coordinate system). Recalling (2.1), we have $ru^i = ikdu^i$, and hence

$$jf(x)j = \ kx\ \ d \quad kjxj\ \ \frac{i}{2}\ \ \frac{1}{2}+2kjxj\ \ \frac{1}{2}+2k\,\mathrm{diam}\ \ ;$$

so that

$$kfk_{L^2(\ )} \quad L^{1=2}\ \ \frac{1}{2}+2k\,\mathrm{diam}\ \ ;\quad k>0: \tag{4.6}$$

Inserting (4.5) and (4.6) into (4.4), the result follows. □

We are now ready to state and prove the main result of this section.

Theorem 4.3. *For all $k_3 > 0$, if is a star-like polygon then*

$$M := \sup_{x2D}ju(x)j \quad C_3(kL)^{1=2}\log^{1=2}(2+kL\ );\quad k \quad k_3;$$

where the constant $C_3 > 0$ depends only on k_3 and , speci cally

$$C_3 = (k_3L)^{\ 1=2}\log^{\ 1=2}(2+k_3L\ ) + \frac{C_2n_s^{1=2}}{\mathrm{ess\,inf}_{x2}\ (x\ \ n(x))}\ \ k_3{}^{\ 1}+4\,\mathrm{diam}\ \ ;$$

where C_2 2:65 is the constant from L6.2267d [(is)aL6.226Td .6.54 -5

5. *hp* Approximation Space and Best Approximation Results. We are now ready to design an approximation space $V_{N;k}$ $L^2(\ )$ to represent

$$'(s) := \frac{1}{k} \frac{@u}{@n}(x(s)) \quad (x(s)) \quad ; \quad s \in [0; L]; \tag{5.1}$$

based on (3.2). Here N denotes the total number of degrees of freedom in the method (to be elucidated later), and the subscript k on $V_{N;k}$ serves to illustrate that our hybrid approximation space depends explicitly on the wavenumber k. The function $'$, which we seek to approximate, can be thought of as the difference between $@u=@n$ and its "Physical Optics" approximation (recall Remark 3.1), scaled by $1=k$ so that $'$ is nondimensional (cf. [14]). Instead of approximating $'$ directly by conventional piecewise polynomials, on each side $_j$, $j = 1;:::;n_s$, we instead use the representation (3.2) with $v_j^+(s \quad t_{j\ 1})$ and $v_j(t_j \quad s)$, $s \in [t_{j\ 1}; t_j]$, replaced by piecewise polynomials supported on overlapping geometric meshes, graded towards the singularities at P_j and P_{j+1} respectively.

Definition 5.1. *Given $A > 0$ and an integer $n > 0$ we denote by $G_n(0;A)$ the geometric mesh on $[0;A]$ with n layers, whose meshpoints x_i are defined by*

$$x_0 := 0; \qquad x_i := \ ^{n\ i}A; \quad i = 1;2;:::;n;$$

where $0 < \ < 1$ is a grading parameter. Given a vector $\mathbf{p} \in (\mathbb{N}_0)^n$ we denote by $P_{\mathbf{p};n}(0;A)$ the space of piecewise polynomials on the geometric mesh $G_n(0;A)$ with degree vector $\mathbf{p}$, i.e.

$$P_{\mathbf{p};n}(0;A) := \ : [0;A] \to C : \ _{(x_{i\ 1};x_i)} \text{ is a polynomial of degree less than or equal to } (\mathbf{p})_i;\ i = 1;:::;n\}:$$

In the case where $(\mathbf{p})_i = p$ for all $i = 1;:::;n$, for some integer $p \quad 0$, we write $P_{p;n}(0;A)$ for $P_{\mathbf{p};n}(0;A)$.

A smaller value of $\ $ represents a more severe grading. While the value $= (\sqrt{2} \quad 1)^2 \quad 0{:}17$ is in some sense optimal, [41, p.96], [22], it is common practice to

The regularity results provided by Theorem 3.2 allow us to prove that, under appropriate assumptions on the choices of N_j and $\mathbf{p}_j$, the best approximation error in approximating $'$ by an element of $V_{N;k}$ decays exponentially as the maximum degree of the approximating polynomials increases.

For simplicity of presentation we shall assume henceforth that the degree of polynomial approximation is constant within each mesh, so that

$$(\mathbf{p}_j)_m = p_j ; \qquad m = 1;:::;N_j ; \tag{5.4}$$

for some integers p_j 0, $j = 1;:::;n_s$

where n is the largest $i \in \{1,\dots,n\}$ such that $\frac{\chi_{i-1}}{2} < 1$. Then one can prove best approximation estimates similar to (5.7) and (5.9) in the space $P_{\mathbf{p};n}(0;A)$. For further details see Appendix A, Theorem A.3.

Combining Theorem 5.2 with Theorem 3.2 we can then deduce the following best approximation result:

Theorem 5.4. *Suppose that*

$$N_j \quad c_j\, p_j\,; \tag{5.10}$$

for some $c_j > 0$. Then there exist constants $\hat{C}_j^+ > 0$, depending only on , c and $_j$, and $\hat{C}_j > 0$, depending only on , c and $_{j+1}$, such that

$$\inf_{v \in P_{p_j;N_j}(0;L_j)} \|v_j \quad v\|_{L^2(0;L_j)} \quad \hat{C}_j\, M k^{1=2} \quad (kL_j)^{1=2} \quad {}_j + \log^{1=2}(2 + kL_j) \quad e^{\,p_j \ {}_j}\,;$$

where $_j = \min\ c_j\, j\log\ j\ 1=2 \quad {}_j\ ; \quad > 0$.

Proof. Applying Theorem 5.2 to $g(z) := v_j\ (z=k)$, which, by Theorem 3.2, satisfies the bounds (5.6) with $\hat{C} = C_j\ M k$ and $= {}_j$, and noting that

$$\inf_{v \in P_{p_j;N_j}(0;L_j)} \|v_j \quad v\|_{L^2(0;L_j)} = \frac{1}{k^{1=2}} \inf_{w \in P_{p_j;N_j}(0;kL_j)} \|g \quad w\|_{L^2(0;kL_j)}\,;$$

the result follows. □

We conclude this section with an estimate for the best approximation error associated with the approximation of $'$ on by an element of $V_{N;k}$. We assume here that (5.4) holds, but a similar result holds when the polynomial degree is reduced towards the singularities, as outlined in Remark 5.3 above. Here and in what follows we make the obvious identification between $L^2(\ )$ and $L^2(0;L)$, via the parametrization $x(s)$.

Theorem 5.5. *Suppose that (5.10) holds for each $j = 1,\dots,n_s$. Then, with $p := \max_j\ \{p_j\}$, there exists a constant $C_4 > 0$, depending only on $\{\ _j\}_{j=1}^{n_s}$, and c , and a constant > 0, depending only on $\{\ _j\}_{j=1}^{n_s}$, , and $\{c_j\}_{j=1}^{n_s}$, such that*

$$\inf_{v \in V_{N;k}} \|k'\ \quad v\|_{L^2(\ )} \quad C_4 M k^{\ 1=2} G(k)\, e^{\ p}\ ; \tag{5.11}$$

where

$$G(k) := (1 + kL\ )^{1=2} \quad + \log^{1=2}(2 + kL\ );$$

and $\quad := \min_j\ \{\ _j\}$.

Proof

(described in the next section). Importantly, however, and as we demonstrate in x7 via numerical examples, this issue does not seem to a ect the accuracy of the solution in the domain, the far eld pattern, or indeed the boundary solution when measured in the weaker L^1 norm.

with S_k given by (4.1), and the result follows from Lemma 4.1 and Theorem 6.1. □

An object of interest in applications is the

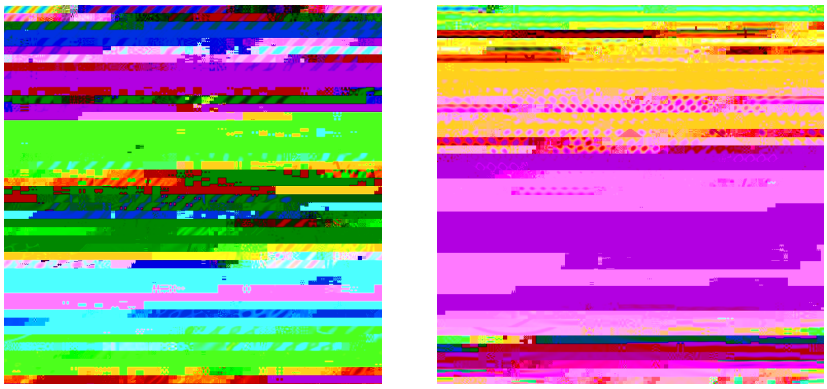

Equilateral triangle Regular pentagon

Fig. 7.1. *Scattering con gurations and plots of the real part of* $u = u^i + u^s$*, for* $k = 10$.

7. Numerical Results. We now present numerical results for the solution of (6.1). We consider two di erent polygonal scatterers, an equilateral triangle and a regular pentagon. In each case the sides of the polygon are of length 2 , so the number of wavelengths per side is equal to k. The scatterers, the incident direction vectors $\mathbf{d}$ (recall (2.1)), the corresponding total elds for $k = 10$, and a circle of radius 2 on which we compute the total eld (see Figures 7.3 and 7.4 below), are plotted in Figure 7.1. For both scatterers we demonstrate exponential decay of the L^2 norm of the error on the boundary as p increases, with only very mild dependence on the wavenumber k, as predicted by (6.2) and (6.3). We also demonstrate how these results extend to the computation of both the solution in the domain and the far eld pattern, error estimates for which are given in (6.4) and (6.8), and we investigate how the accuracy of our results depends on the geometry of the scatterer. The results presented here are computed using the standard combined potential formulation, with $A = A_{k;}$; we make this choice because we wish to demonstrate that our numerical results are entirely consistent with our theoretical predictions, even though we do not yet have a complete theory for this case (since, as discussed in Remark 2.4, Assumption 2.3 has not yet been shown to hold for $A = A_{k;}$). In all of our experiments we take the same degree p of polynomial approximation on each element, and the same number of layers $N_l := 2(p + 1)$ on each graded mesh. According to (5.5), with $N_j = N_l$ and $p_j = p$ for each $j = 1;:::;n_s$, the total number of degrees of freedom is given by

$$N = 4n_s(p + 1)^2: \tag{7.1}$$

Since for each example N depends only on p (through (7.1)), we simplify our presentation by de ning $_p(s) := '_N(s)$. For the purposes of comparison with the theoretical results, we note that in both examples (5.10) is satis ed with $c_j = 2$ for each $j = 1;:::;n_s$.

In Figure 7.2 we plot the relative L^2 and L^1 errors (each on a logarithmic scale) against p, for both examples and for a range of values of k. In each case we take the \exact" reference solution to be that computed with $p = 7$; further veri cation of our method via comparison with solutions computed using the h-version scheme of [14], with a large number of degrees of freedom, has also been performed, but is not reported in detail here. The L^2 and L^1 norms are computed by a high-order composite Gaussian

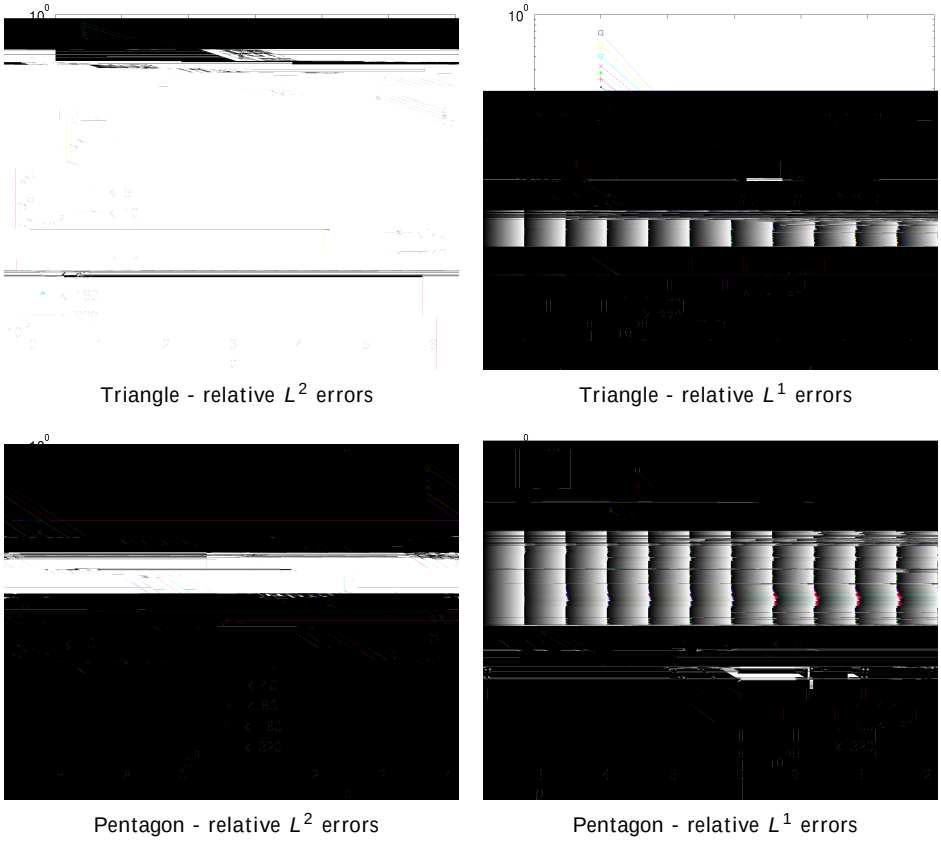

Triangle - relative L^2 errors

Triangle - relative L^1 errors

Pentagon - relative L^2 errors

Pentagon - relative L^1 errors

Fig. 7.2. *Relative L^2 and L^1 errors in boundary solution.*

quadrature scheme on a mesh graded towards the corner singularities; experimental evidence suggests that these calculations are accurate to at least four digits of precision (a far higher accuracy than that achieved by the corresponding quadrature scheme in [14], which used a uniform mesh).

The linear plots in Figure 7.2 clearly demonstrate exponential decay with increasing polynomial degree p, as predicted for the L^2 error by Theorem 6.2. We shall make comparisons between the four plots in Figure 7.2 shortly. However, we rst focus on the .digher accuracyincreas-

k	$\frac{N}{L=}$	$k_{7\ 4k_{L}2(\ )}$		$\frac{k_{7\ 4k_{L}2(\ )}}{k_{7k_{L}2(\ )}}$	$\frac{k_{7\ 4k_{L}1(\ )}}{k_{7k_{L}1(\ )}}$	COND	cpt(s)
5	20.00	1.96 10 ^{1}	-0.40	1.44 10 ^{1}	8.33 10 ^{3}	3.50 10^{2}	621
10	10.00	1.48 10 ^{1}	-0.40	1.55 10 ^{1}	1.24 10 ^{2}	2.77 10^{1}	612
20	5.00	1.12 10 ^{1}	-0.40	1.66 10 ^{1}	1.58 10 ^{2}	3.51 10^{1}	600
40	2.50	8.50 10 ^{2}	-0.40	1.78 10 ^{1}	1.74 10 ^{2}	4.60 10^{1}	691
80	1.25	6.44 10 ^{2}	-0.40	1.91 10 ^{1}	1.83 10 ^{2}	6.12 10^{1}	665
160	0.63	4.88 10 ^{2}	-0.40	2.04 10 ^{1}	1.91 10 ^{2}	8.27 10^{1}	648
320	0.31	3.70 10 ^{2}	-0.40	2.19 10 ^{1}	2.02 10 ^{2}	1.12 10^{2}	746
640	0.16	2.80 10 ^{2}	-0.38	2.35 10 ^{1}	2.06 10 ^{2}	3 [(1) 10 ^{2}	

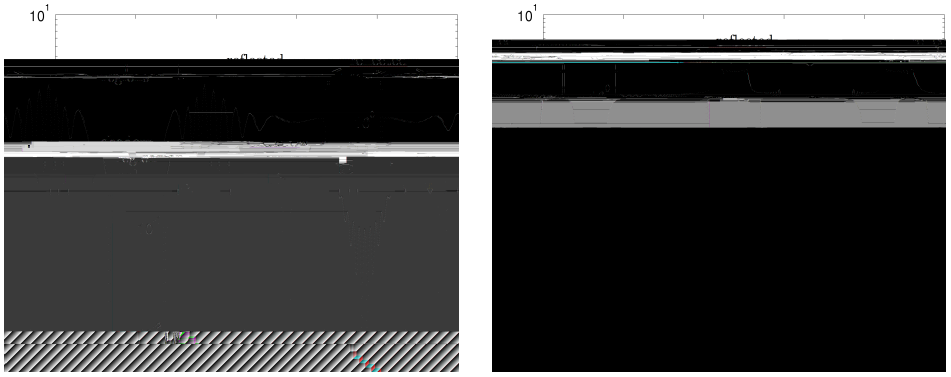

$k = 10$ $k = 160$

Fig. 7.3. *Total field for the triangle, evaluated on the circle of Figure 7.1.*

the solution on the boundary remains bounded, even as $_j \to 2$. The plots in Figure 7.2 reflect this, with the errors in the L^1 norm being much smaller than the corresponding L^2 errors, and this difference being particularly pronounced for the scatterer with sharper corners (the triangle). Moreover, there is little difference in either the magnitude or rate of decay of the L^1 errors between the two examples, which suggests that the L^1 error is not significantly affected by corner angles. We return to this observation at the end of the paper.

We now turn our attention to the approximation of $u(\mathrm{x})$, $\mathrm{x} \in D$, and of the far field pattern F (often the quantities of real interest in scattering problems). As might be expected of linear functionals of the boundary solution, we find that the errors in $u(\mathrm{x})$ and F are, in general, much smaller than the relative errors in $'$. Moreover, the sensitivity to the corner angles seen in the L^2 errors in $'$ does not seem to be present in the approximations of $u(\mathrm{x})$ and F.

To investigate the accuracy of our solution in the domain, we compute the solution on a circle of radius 2 surrounding the scatterer, as illustrated in Figure 7.1. To allow easy comparison between different discretizations, noting again that for each example N depends only on p (recall (7.1)), we denote the solution on the circles (with a slight abuse of notation) by $u_p(t) := u_N(\mathrm{x}(t))$, $t \in [0; 2\ ]$, where $t = 0$ corresponds to the direction from which u^i is incident. Plots of $|u_7(t)|$ (i.e. the total field on the circle as computed with our finest discretization) for the equilateral triangle, for $k = 10$ and $k = 160$, are shown in Figure 7.3. The shadow region and the regions in which specularly reflected waves are present are indicated (compare Figure 7.3 with Figure 7.1).

In Figure 7.4 we plot for both examples the relative maximum error on the circle,

$$\frac{\max_{t \in [0;2\ ]} |u_7(t) - u_p(t)|}{\max_{t \in [0;2\ ]} |u_7(t)|},$$

computed over 10000 evenly spaced points in $[0; 2\ ]$, for $k = 10$, $k = 40$, and $k = 160$. The exponential decay with respect to increasing p predicted by Theorem 6.3 is clear for both examples (note the logarithmic scale on the vertical axes). Moreover, for fixed p, the relative maximum error seems to be, if anything, decreasing with increasing k, suggesting that the theoretical error bound (6.4) in Theorem 6.3 is not sharp in terms of its k dependence. As alluded to above, the errors in the domain are much

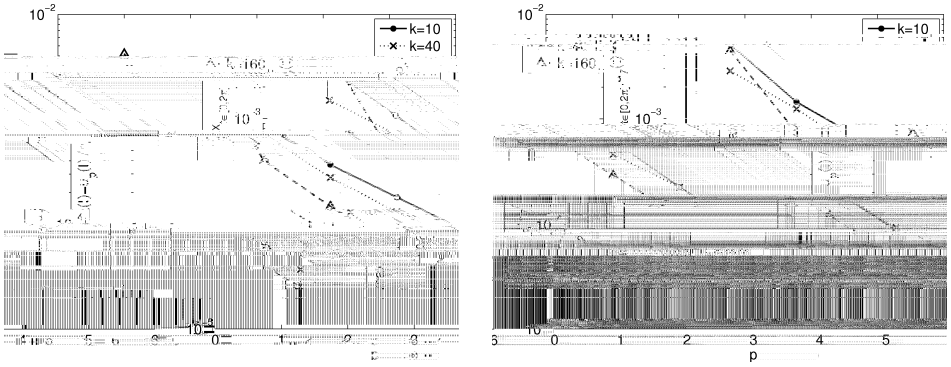

Triangle Pentagon

Fig. 7.4. *Relative maximum errors on the circles of Figure 7.1.*

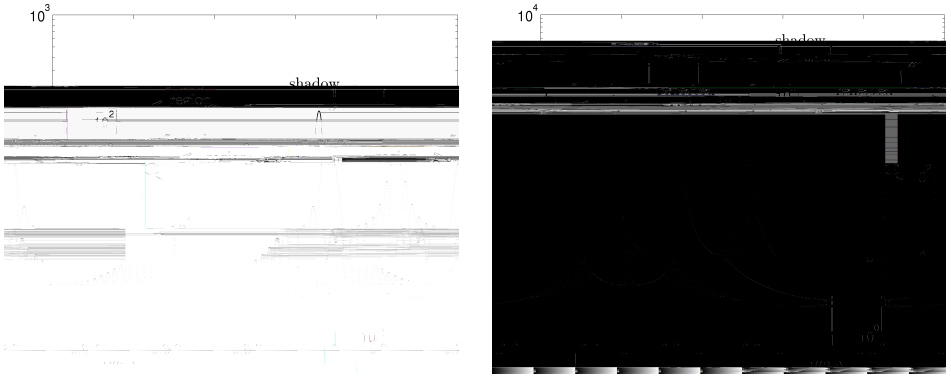

k=10 k=160

Fig. 7.5. *Far eld patterns for the triangle.*

smaller than the relative errors in the computation of the boundary data in Figure 7.2, and, importantly, for xed k and p the errors for the two examples are of similar magnitude. This suggests that the bound (6.4) in Theorem 6.3 is not sharp in terms of its dependence on the corner angles, either.

Finally, we compute our approximation to the far eld pattern (6.7). As above, to allow easy comparison between di erent discretizations we denote (again with a slight abuse of notation) $F_p(t) := F_N(\hat{x}(t))$, $t \in [0; 2\pi]$, where $t = 0$ again corresponds to the direction from which u^i is incident. Plots of $|F_7(t)|$ (i.e. the far eld pattern as

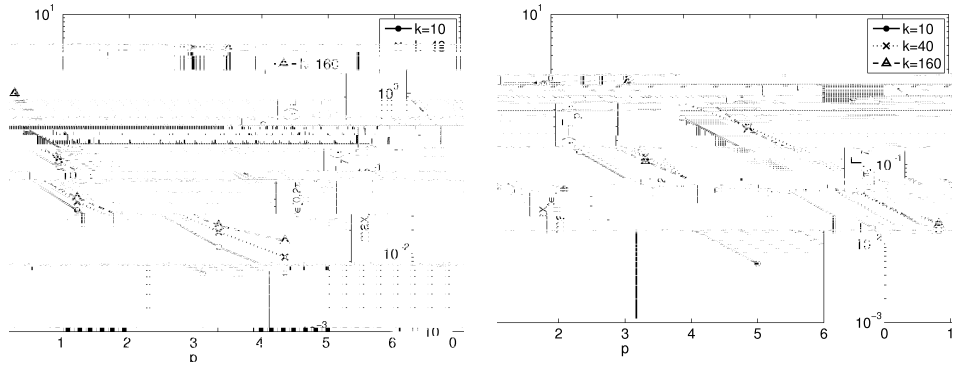

Fig. 7.6. *Absolute maximum errors* $kF_7 \quad F_p k_{L^1(0;2)}$ *in the far eld pattern.*

and p the errors are comparable in magnitude for the two examples, suggesting that, as for the solution in the domain, the bound (6.8) may not be optimal in terms of its dependence on the corner angles, either.

In summary, our numerical examples demonstrate that the predicted exponential convergence of our *hp* scheme is achieved in practice. Moreover, for a xed number of degrees of freedom, the accuracy of our numerical solution appears to deteriorate only very slowly (or not at all) as the wavenumber k increases. In fact, our results lead us to conjecture that *the theoretical error bounds provided by Corollary 6.2 and Theorems 6.3 and 6.4 are not sharp in their k dependence*. In particular, we believe that this is partly due to the lack of sharpness of our estimate for M derived in *x*4; indeed, we conjecture (cf. Remark 3.3) that $M = O(1)$ as $k \; ! \; 1$, but, as yet, we do not have a proof of this result.

We also conjecture that *the theoretical error bounds provided by Theorems 6.3 and 6.4 are not sharp in their dependence on the corner angles of the polygon*. To explain this, we recall that our error estimates for the approximation of u by u_N, (6.4), and of F by F_N, (6.8), were derived via the Cauchy-Schwarz inequality and our L^2 estimates for $' \quad '_N$, (6.2) and (6.3), which we know to blow up to in nity if one (or more) interior corner angle(s) tend to zero, re ecting that, in this limit, $'$ ceases to be in $L^2(\ )$. Our choice of $L^2(\ )$ as the space for error analysis is motivated by the very recent results in [42], where coercivity was established with frequency independence for a second kind BIE formulation. One way to obtain error estimates

the form presented here, appropriately modified versions of Lemma 2.1, Lemma 2.2 and Assumption 2.3 would also be required. We do not explore these issues further here, except to say that the difficulty in dealing with the singularities when the corner angles are sharp is unrelated to considerations regarding the oscillatory nature of the solution, which form the main focus of this paper.

8. Acknowledgements. The authors thank S. N. Chandler-Wilde for many helpful discussions and A. Twigger for assistance with computing numerical results.

REFERENCES

[1] *Digital Library of Mathematical Functions*. National Institute of Standards and Technology, from http://dlmf.nist.gov/, release date: 2010-05-07.

[2] S. Arden, S. N. Chandler-Wilde, and S. Langdon, *A collocation method for high-frequency scattering by convex polygons*

[20] V. Dominguez, I. G. Graham, and V. P. Smyshlyaev, *A hybrid numerical-asymptotic boundary integral method for high-frequency acoustic scattering*, Numer. Math., 106 (2007), pp. 471{510.
[21] M. Ganesh and S. C. Hawkins,

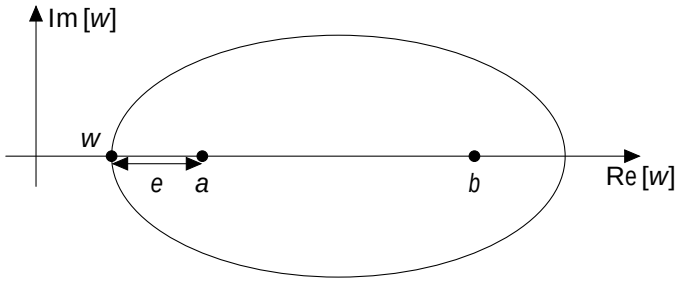

Fig. A.1. *Ellipse parameters.*

Lemma A.2. *Suppose that a function g is analytic and bounded in* $E_{a;b;r}$ *for some* $1 < a < b < 1$ *and* $r > b \quad a$. *Then*

$$\inf_{v2P_p(a;b)} kg \quad vk_{L^1(a;b)} \quad \frac{2}{1} \quad {}^{p} kgk_{L^1(E_{a;b;r})}; \tag{A.2}$$

where

$$= \frac{1}{b \quad a} \quad r + \sqrt[p]{r^2 \quad (b \quad a)^2} \quad > 1: \tag{A.3}$$

Using this result we can prove Theorem 5.2.

Proof. (Proof of Theorem 5.2.) Part (ii) is clearly a trivial consequence of part (i). To prove (i), it is convenient to introduce the notation

$$E_i := \inf_{v2P_p(x_i \quad 1;x_i)} kg \quad vk_{L^1(x_i \quad 1;x_i)}; \tag{A.4}$$

$$I_i := \inf_{v2P_p(x_i \quad 1;x_i)} kg \quad vk_{L^2(x_i \quad 1;x_i)}; \tag{A.5}$$

for each $i = 1;2;:::;n$. We then have

$$\inf_{v2P_{p;n}(0;A)} kg \quad vk_{L^0;A}$$

[(i)]TJ/F8 9.3738Td [(L)]TJ/858-

If $n \geq 2$, then for $i = 2;3;\ldots;n$, g is analytic and bounded in the half plane $\mathrm{Re}[z] > \frac{x_{i-1}}{2}$. With reference to Figure A.1, we note that for the general ellipse $E_{a;b;r}$ of Definition A.1, setting $w = w^*$ reveals that $r = 2e + (b - a)$. Hence the largest ellipse $E_{x_{i-1};x_i;r_i}$ lying inside the half-plane $\mathrm{Re}[z] > \frac{x_{i-1}}{2}$ has $r_i = (x_i - x_{i-1}) + x_{i-1} = x_i$, so Lemma A.2 implies that

$$E_i \leq \left(\frac{2B_i}{\rho - 1}\right)^p; \qquad i = 2;3;\ldots;n; \tag{A.10}$$

where $B_i := \|g\|_{L^1(E_{x_{i-1};x_i;r_i})}$ and

$$\rho := \frac{1}{x_i - x_{i-1}}\left(r_i + \sqrt{r_i^2 - (x_i - x_{i-1})^2}\right) = \frac{1}{1-\delta}\left(1 + \sqrt{p - p\delta}\right) > 1. \tag{A.11}$$

Hence

$$I_i^2 \leq \left(\frac{4B_i^2(x_i - x_{i-1})}{(\rho - 1)^2}\right)^{2p}; \qquad i = 2;3;\ldots;n. \tag{A.12}$$

Now define n^* to be the largest $i \in \{1;\ldots;n\}$ such that $\frac{x_{i-1}}{2} < 1$, i.e.

$$n^* := \begin{cases} \left\lfloor \dfrac{\log A - \log 2}{j \log \rho} \right\rfloor; & A = 2 - \delta < 1; \\ n; & \text{otherwise.} \end{cases} \tag{A.13}$$

Then

$$B_i \leq \begin{cases} C\left(\frac{x_{i-1}}{2}\right) = C\left(\frac{\rho^{n^*-i+1}A}{2}\right); & 2 \leq i \leq n^*; \\ C\left(\frac{x_{i-1}}{2}\right)^{1/2} = C\left(\frac{\rho^{n^*-i+1}A}{2}\right)^{1/2}; & n^* + 1 \leq i \leq n. \end{cases} \tag{A.14}$$

Hence if $n \geq 2$, then for $i = 2;\ldots;n$ we have

$$B_i^2(x_i - x_{i-1}) \leq C^2\left(\frac{\rho^{n^*-i+1}A}{2}\right)^2 \rho^{n^*-i}A(1-\delta) = \frac{2^2 C^2 \rho^{2n^*-2i}A^2(1-\delta)}{2}; \tag{A.15}$$

so that

$$I_i^2 \leq \left(\frac{2^{2+2}C^2\rho^{2n^*-2i}A^2(1-\delta)}{\rho^2(\rho-1)^2}\right)^{2p}; \qquad i = 2;\ldots;n. \tag{A.16}$$

By the definition of n^*, $\frac{x_{n^*-1}}{2} = \frac{A\rho^{n^*-n^*+1}}{2} < 1$, so $\rho^{n^*-i}A = \rho^{n^*-n^*+1}A\rho^{n^*+1-i} < 2\rho^{2n^*+1-i}$, and

$$\sum_{i=2}^{n^*} \rho^{n^*-i}A^{1/2} \leq (2\rho^2)^{1/2}\sum_{i=2}^{n^*} e^{-2(n^*+1-i)\#} \leq \frac{(2\rho^2)^{1/2}e^{-2\#}}{1-e^{-2\#}}; \tag{A.17}$$

with $\#$ defined as in (A.8). Hence

$$\sum_{i=2}^{n^*} I_i^2 \leq C^2 D_2^{2p}; \tag{A.18}$$

where

$$D_2(\ ;\ ) = \frac{2^{2+2}\ (2\quad ^2)^{1\ \ 2}\ e^{\ 2\#}(1\quad)}{(1\quad e^{\ 2\#})^{\ 2}\ (\quad 1)^2} = \frac{8^{\ \ 1\ \ 4}\ (1\quad)}{(1\quad ^{1\ \ 2})(\quad 1)^2}: \qquad \text{(A.19)}$$

If $n\quad n\quad 1$ (i.e. $A=2\quad 1$), then for $i = n\ + 1;:::;n$ we have the simpler result

$$B_i^2(x_i\quad x_{i\ \ 1}) = \hat{C}^2\ \ \frac{^{n\ \ i+1}A}{2}\ \ ^{1\ \ n\ \ i}A(1\quad) = \frac{2\hat{C}^2(1\quad)}{\quad}; \qquad \text{(A.20)}$$

so that

$$I_i^2\quad \frac{8\hat{C}^2(1\quad)}{(\quad 1)^2}\quad ^{2p}; \qquad i = n\ + 1;:::;n: \qquad \text{(A.21)}$$

Hence

$$\sum_{i=n\ +1} I_i^2\quad (n\quad n\ )\hat{C}^2 D_3\quad ^{2p}; \qquad \text{(A.22)}$$

where

$$D_3(\ ) = \frac{8(1\quad)}{(\quad 1)^2}: \qquad \text{(A.23)}$$

Note also that since $A=2$ I n In this case, we can bound

(i) there exists a constant $C' > 0$*, depending only on* $\quad$ *and* $\quad$*, such that the best* L^2 *approximation error in* $P_{\mathbf{p};n}(0;A)$ *satisfies*

$$\inf_{v \in P_{\mathbf{p};n}(0;A)} \|g - v\|_{L^2(0;A)} \quad C'\hat{C} \quad A^{1=2} \quad e^{\quad n\#} + (2 + A)^{1=j \log \quad j} e^{\quad n} + \log^{1=2}(2 + A) e^{\quad p} \quad ; \qquad \text{(A.27)}$$

where $\#$ *and* $\quad$ *are as defined in Theorem 5.2, and* $\quad = \min\{\#=2; p = n\}$*;*

(ii) furthermore, if n *is chosen such that* $n \quad cp$ *for some constant* $c > 0$*, th*

$$\inf_{v \in P_{\mathbf{p};n}(0;A)} \|g - v\|_{L^2(0;A)} \quad {}^{0}\hat{C} \quad A^{1}$$

where

$$D_4^{\prime} = \max\left(D_1; D_2^{\prime}; \frac{D_3}{j \log j} \right); \tag{A.36}$$

giving

$$\inf_{v \in P_{\mathbf{p};n}(0;A)} \|g - v\|_{L^2(0;A)} \leq C^{\prime} \hat{C} A^{1/2} \left(e^{-n\#} + e^{-n} + \log^{1/2}(2 + A) e^{-p} \right); \tag{A.37}$$

where $C^{\prime} := \sqrt{D_4^{\prime}}$. Finally, we obtain (A.27) by noting that

$$n \geq n \geq \frac{\log(2 + A)}{j \log j}; \tag{A.38}$$

which follows from (A.24) for $A/2 \geq 1$ and the fact that $n = n$ for $A/2 < 1$.

Part (ii) follows trivially from part (i) and the fact that $n = \min\{n\#/2; np = n\} \geq p \min\{c\#/2; g\}$. □